Published in final edited form as:
Mech Mater. 2012 January ; 44: . doi:10.1016/j.mechmat.2011.08.005.

Bi-material attachment through a compliant interfacial system at the tendon-to-bone insertion site

Y.X. Liu[a], **S. Thomopoulos**[b], **V. Birman**[c], **J.-S. Li**[d], and **G.M. Genin**[a,*]

[a]Department of Mechanical Engineering and Materials Science, Washington University, St. Louis, MO 63130, USA

[b]Department of Orthopaedic Surgery, Washington University School of Medicine, St. Louis, MO 63110, USA

[c]Engineering Education Center, Missouri University of Science and Technology, One University Blvd., St. Louis, MO 63121, USA

[d]Department of Electrical and Systems Engineering, Washington University, St. Louis, MO 63130, USA

Abstract

The attachment of tendon to bone, one of the greatest interfacial material mismatches in nature, presents an anomaly from the perspective of interfacial engineering. Deleterious stress concentrations arising at bi-material interfaces can be reduced in engineering practice by smooth interpolation of composition, microstructure, and mechanical properties. However, following normal development, the rotator cuff tendon-to-bone “insertion site” presents an interfacial zone that is more compliant than either tendon or bone. This compliant zone is not regenerated following healing, and its absence may account for the poor outcomes observed following both natural and post-surgical healing of insertion sites such as those at the rotator cuff of the shoulder. Here, we present results of numerical simulations which provide a rationale for such a seemingly illogical yet effective interfacial system. Through numerical optimization of a mathematical model of an insertion site, we show that stress concentrations can be reduced by a biomimetic grading of material properties. Our results suggest a new approach to functional grading for minimization of stress concentrations at interfaces.

Keywords

Stress concentrations; Material optimization; Tendon-to-bone attachment; Enthesis

1. Introduction

Connecting dissimilar materials is a fundamental challenge because of stress concentrations that can arise at their interface (Williams, 1952). Interfacial stress concentrations can contribute to material failures at levels of mechanical loads that are too small to cause failure in either material individually (Hutchinson and Suo, 1992). “Functionally graded” material systems that interpolate spatially between properties of two materials are often considered to reduce stress concentrations in engineering and medical applications, ranging from

*Corresponding author. Address: Department of Mechanical Engineering and Materials Science, Campus Box 1185, Washington University in St. Louis, St. Louis, MO 63130, USA. Tel.: +1 314 935 5660; fax: +1 314 935 4014. genin@wustl.edu. .

semiconductor thin films to prosthetic joints and limbs (Birman and Byrd, 2007; Suresh and Mortensen, 1998; Tersoff and LeGoues, 1994).

In nature, a graded material exists between the unmineralized ("soft") and mineralized ("hard") tissues (Thomopoulos et al., 2003; Stouffer et al., 1985), for example, at the shoulder's rotator cuff tendon-to-bone attachment (Fig. 1). Here, tendon attaches to bone through a fibrocartilaginous transition zone ("insertion site") that presents a continuous spatial grading in mineralization and organization of the underlying collagen fibers (Wopenka et al., 2008). Although data and models are sparse, current data suggest that this attachment mechanism might exist in other tensile connections such as ligaments (Moffat et al., 2008) and menisci (Villegas et al., 2007), but not in compressive osteochondral connections (Ferguson et al., 2003). Whereas engineering practice would be to interpolate between the mechanical properties of tendon and bone, recent experimental evidence indicates that grading at the rotator cuff insertion site produces a soft tissue region that is more compliant than either tendon or bone (Genin et al., 2009).

The interface between tendon and bone develops following birth, and matures only after weight-bearing and increased muscle loading (Das et al., 2011; Thomopoulos et al., 2007, 2010). In contrast to the developmental process, a functionally graded transition is not regenerated at the healing tendon-to-bone insertion. Rather, scar tissue fills the repair site, resulting in an abrupt interface that lacks a compliant band between the tendon and the bone (Thomopoulos et al., 2003). Surgical repair of tendon-to-bone attachment at the rotator cuff is therefore prone to re-injury, with failure rates up to 94% for rotator cuff reattachment (Galatz et al., 2004). Understanding the counter-intuitive biophysics of the natural attachment (i.e., a compliant zone at the interface between the disparate materials) is important for medical practice and for biomimetic design.

The hypothesis that the grading found at the insertion site reduces stress concentrations has been suggested (Benjamin et al., 2002; Thomopoulos et al., 2006), but evidence that this unusual attachment scheme actually reduces stresses has not been reported. Here, we show through numerical optimization of a mathematical model of a rotator cuff insertion site that a qualitatively biomimetic material grading can reduce or even eliminate stress concentrations in a model of the rotator cuff insertion site. Fields in the vicinity of an interface are shown to depend strongly upon the local material grading. Taken in the context of hierarchical structural adaptation to mitigate stress concentrations in biological systems, results have implications for the design of engineering interfaces, surgical techniques, and surgical grafts that guide tissue development following insertion site repair.

2. Mathematical model and optimization methods

The effects of material stiffness grading on the stress field at the attachment of tendon to bone were assessed by studying an idealization of the rotator cuff insertion site (Fig. 1). The mathematical model involved axisymmetric linear elasticity (Fig. 2), and in all cases studied involved an isotropic bone core within a cylindrically orthotropic tendon. This is a reasonable first-order approximation of physiologic loading in the rotator cuff tendons, as evidenced by the anatomy of the rotator cuff viewed in the sagittal plane (Fig. 1). Note that while the humeral head contains insertion sites for several tendons, these insertion sites do overlap to a degree (Fig. 1). Symmetry arguments suggest that this axisymmetric model is most accurate at the midplane passing through the supraspinatus.

The efficacy of a graded insertion was assessed by comparing the results of optimizations to several comparison cases. In each instance, a different interfacial system was chosen to connect an orthotropic tendon to an isotropic bone, and a stress analysis was performed. The

methods for the stress analysis are presented below, followed by detailed methods for the optimizations and comparison cases.

2.1. Stress analysis

The stress field within the model was obtained by assuming all out-of-plane stresses to be zero, as is reasonable for a two-dimensional idealization of tendon, and by assuming all deformations to be small (Matyas et al., 1995). The assumptions of isotropy in bone and orthotropy in tendon are well justified based upon experiment (Fung, 1993). A linear approximation was used for material properties, which is acceptable for the mineralized and partially mineralized tissues near the bone where peak stress concentrations are likely to arise (Genin et al., 2009); at all other points, the moduli must be understood as incremental tangent moduli for a specific loading level (Prager, 1969). The insertion site and tendon were modeled using M concentric and perfectly bonded bands of cylindrically orthotropic material, with the outer radius of the mth band denoted by R_m. The in-plane mechanical properties of the mth band were described by three constants: the elastic moduli in the radial and tangential directions, $E_r^{(m)}$ and $E_\theta^{(m)}$, respectively, and the Poisson's ratio $\nu_{r\theta}^{(m)}$ that indicates the degree of tangential contraction associated with radial stretching. The other Poisson's ratio depends upon the specified material constants of the band:

$$\nu_{\theta r}^{(m)} = \nu_{r\theta}^{(m)} E_\theta^{(m)} / E_r^{(m)}$$

The radial and tangential stresses in the mth orthotropic band due to radial compressive stresses q_m and q_{m-1} applied at the outer and inner interfaces of the mth band, respectively, are (Lekhnitskii, 1968):

$$\begin{aligned}
\sigma_r^{(m)}(r) = {} & \frac{q_{m-1}c_m^{k_m+1}}{1-c_m^{2k_m}}\left[\left(\frac{r}{R_m}\right)^{k_m-1} - \left(\frac{R_m}{r}\right)^{k_m+1}\right] \\
& + \frac{q_m}{1-c_m^{2k_m}}\left[-\left(\frac{r}{R_m}\right)^{k_m-1} + c_m^{2k_m}\left(\frac{R_m}{r}\right)^{k_m+1}\right] \\
\sigma_\theta^{(m)}(r) = {} & \frac{q_{m-1}c_m^{k_m+1}}{1-c_m^{2k_m}}k_m\left[\left(\frac{r}{R_m}\right)^{k_m-1} + \left(\frac{R_m}{r}\right)^{k_m+1}\right] \\
& - \frac{q_m}{1-c_m^{2k_m}}k_m\left[\left(\frac{r}{R_m}\right)^{k_m-1} + c_m^{2k_m}\left(\frac{R_m}{r}\right)^{k_m+1}\right]
\end{aligned} \tag{1}$$

where r is the radial coordinate measured from the center of the bone, $c_m = R_{m-1}/R_m$, and $k_m = \sqrt{E_\theta^{(m)}/E_r^{(m)}}$. The stress field in the isotropic bone depended only on the stress at its outer boundary, $\sigma_r = \sigma_\theta = -q_o$. The continuity requirement for radial displacements along the boundaries of the adjacent bands $u_r^{(m)}(r=R_m) = u_r^{(m+1)}(r=R_m), m=1,2,\ldots,M-1$ and the bone-to-insertion boundary $u_r^{(0)}(r=R_o) = u_r^{(1)}(r=R_o)$ yielded M equations for the M unknown values of q_m:

$$\begin{aligned}
q_o &= 2q_1 k_1 c_1^{k_1-1}\left(\frac{E_\theta^{(1)}}{E_{\text{bone}}}(1-\nu_{\text{bone}})\left(1-c_1^{2k_1}\right) + \left[\left(1+c_1^{2k_1}\right)k_1 + \left(1-c_1^{2k_1}\right)\nu_{\theta r}^{(1)}\right]\right)^{-1} \\
0 &= q_o R_o \alpha_1 + q_1 R_1 \beta_1 + q_2 R_2 \alpha_2 \\
0 &= q_1 R_1 \alpha_2 + q_2 R_2 \beta_2 + q_3 R_3 \alpha_3 \\
&\vdots \\
0 &= q_{M-2} R_{M-2} \alpha_{M-1} + q_{M-1} R_{M-1} \beta_{M-1} + \sigma_M R_M \alpha_M
\end{aligned} \tag{2}$$

where $\sigma_M = -p$ is the inward radial stress applied to the outermost boundary of the band of tendon, and

$$\begin{aligned}\alpha_m = & \frac{2k_m c_m^{k_m}}{E_\theta^{(m)}\left(1-c_m^{2k_m}\right)} \\ \beta_m = & \frac{1}{E_\theta^{(m)}}\left[\nu_{\theta r}^{(m)} - k_m \frac{\left(1+c_m^{2k_m}\right)}{\left(1-c_m^{2k_m}\right)}\right] \\ & -\frac{1}{E_\theta^{(m+1)}}\left[\nu_{\theta r}^{(m+1)} + k_{m+1}\frac{\left(1+c_{m+1}^{2k_{m+1}}\right)}{\left(1-c_{m+1}^{2k_{m+1}}\right)}\right]\end{aligned} \quad (3)$$

Note that Lekhnitskii (1968) published a related solution for the displacement field in a pressurized, cylindrically orthotropic, layered pipe. However, the Lekhnitskii solution can be shown to be incorrect by reduction to the isotropic solution.

In analyses for which gradients of material properties were studied and optimizations were performed, the domain between tendon and bone was divided into $M - 1 = 500$ bands. five hundred bands were sufficient to ensure convergence for all conditions tested. In all analyses, the two constants describing the mechanical properties of the bone were $E_{bone} = 20$ GPa and $\nu_{bone} = 0.3$, and the three constants describing those of tendon were $E_r = 450$ MPa, $E_\theta = 45$ MPa, and $\nu_{r\theta} = 3$ (Lynch et al., 2003; Stabile et al., 2004). While these latter values are for ligaments rather than tendons, they represent the best data available, and, despite morphological and compositional variations unique to the rotator cuff (Blevins et al., 1997), the mechanical properties of rotator cuff tendons are of the same order as those of other tendons and ligaments of the body.

Dimensions (Fig. 2) were chosen to represent the rotator cuff of the humeral head. The size of the outer band of tendon was chosen to ensure that stress gradients at the outer boundary were sufficiently small to discount effects of the outer boundary on the stress distribution within the insertion.

2.2. Comparison cases

To assess the efficacy of material grading, five hypothetical comparison cases were studied. The first four involved no optimization of material properties. The first was a case in which tendon connected to the bone without an interfacial zone, so that the white region in Fig. 2 assumed the mechanical properties of tendon. The second case was a fully mineralized insertion site, in which the white region in Fig. 2 assumed mechanical properties of bone; note that this case differs from case 1 because of the length scale in the model associated with the size of the insertion site.

The third case was the intuitive engineering approach to reducing a stress concentration, which involves functional grading that interpolates between tendon and bone. The data of Moffat et al. (2008) suggest that this might be relevant physiologically for a ligament to bone insertion site loaded in compression. To assess the efficacy of this approach, material properties $E_r^{(m)}$ and $E_\theta^{(m)}$ were interpolated linearly with respect to r between those of tendon and bone. Poisson's ratio $\nu_{r\theta}$ was fixed at 0.3 throughout the insertion as the simplest approach to satisfying for all E_r and E_θ the thermodynamic constraint $|\nu_{r\theta}| \leq \sqrt{E_r/E_\theta}$; in the $\nu_{r\theta}$ was equal to 3.

The fourth case involved a sigmoidal interpolation of $E_r^{(m)}$ and $E_\theta^{(m)}$ between the values in tendon and those in bone, again with Poisson's ratio $\nu_{r\theta}$ fixed at 0.3 throughout the insertion. The objective of these was to determine whether a smooth, monotonic, non-optimized interpolation could improve upon the above comparison cases. The sigmoidal function chosen was a weighted logistic function centered at the midpoint of the insertion:

$$\frac{E_\theta^{(m)}}{E_{bone}} = \frac{E_\theta^{tendon}}{E_{bone}} + \frac{1 - E_\theta^{tendon}/E_{bone}}{1 + \exp\left(-6\omega\left(1 - 2x^{(m)}\right)\right)} \quad (4)$$

in which $x^{(m)} = (0.5(R_m + R_{m-1}) - R_o)/R_M - R_o)$. An analogous interpolation was used for E_r.

The final comparison case involved optimization of a model in which the insertion site was assigned mechanical properties that were spatially uniform. The efficacy of a discrete tissue interface of this character is relevant physiologically, reflecting a different model of the insertion site as being comprised of four distinct zones (Benjamin et al., 2002). In the model considered here, the insertion site (white region, Fig. 2) was assigned spatially uniform orthotropic material properties. Stress concentrations (peak stress within the model, normalized by the magnitude of the applied stress) were calculated for values of insertion site moduli E_r and E_θ varying from approximately zero to the elastic modulus of bone. At each value of E_r and E_θ, the Poisson's ratio $\nu_{r\theta}$ of the insertion site was optimized using standard gradient methods to minimize the peak radial stress.

2.3. Optimizations

A series of optimization trials were performed to evaluate whether a smooth, continuous functional grading within the insertion site could prove more effective than these comparison cases. $E_r(r)$, $E_\theta(r)$, and $\nu_{r\theta}(r)$ were allowed to vary independently within the insertion site, subject at each radial position to the thermodynamic constraints described below and to the physiologic constraint that neither $E_r(r)$ nor $E_\theta(r)$ could exceed E_{bone}. These distributions were optimized to reduce peak radial stress, peak strain energy density, peak hydrostatic stress, or peak radial strain within the model.

Spatial variations of insertion site moduli were continuous according to $N = 15$ degree Bezier interpolation functions, with $N + 1 = 16$ control points. Moduli at the tendon and bone extremities of the insertion site were matched to those of tendon and bone, respectively, to enforce continuity, resulting in a total of $(16 - 2) \times 3 = 42$ optimization variables. Bezier interpolation functions were chosen because, by constraining values at control points to remain positive, the constraint that moduli $E_r(r)$ and $E_\theta(r)$ be positive at all points could be enforced. Higher degree Bezier functions provided higher flexibility at higher computational cost; lower degree functions had insufficient flexibility; $N = 15$ provided sufficient flexibility to eliminate stress concentrations at reasonable computational cost.

In each optimization, design variables at these control points were varied to minimize one of several optimization criteria. Standard gradient-based minimization algorithms implemented in the Matlab (Natick, MA) environment were employed (Press et al., 2007). The gradient-based algorithm stalled frequently in local minima. In such cases, a genetic approach was applied until the local minimum had been exited (Huang et al., 2003). Minimization using the gradient-based algorithm was then resumed. The genetic optimizations ended either when they improved upon the results of the gradient-based approach by 1% or after 20 generations. While we could not be certain that this criterion provided a global minimum, successive simulations in each case studied converged upon local minima that were similar and independent of starting conditions.

2.4. Enforcement of thermodynamic constraints

Three thermodynamic constraints had to be enforced throughout the insertion site. First was the requirement that all moduli $E_r^{(m)}$ and $E_\theta^{(m)}$ must be greater than zero. Second,

$|\nu_{r\theta}| \leq \sqrt{E_r/E_\theta}$ (Lekhnitskii, 1968). Third, the volumetric dilatation, ΔV/V, must be positive for a positive tension, p; satisfying the second constraint will always satisfy this third constraint for a transversely isotropic material with $E_z = E_\theta$. The constraint follows from the constitutive equation:

$$\frac{\Delta V}{V} = \varepsilon_{rr} + \varepsilon_{\theta\theta} + \varepsilon_{zz} = p\left(\frac{1}{E_r}(1 - 4\nu_{r\theta}) + \frac{2}{E_\theta}(1 - \nu_{z\theta})\right) \quad (5)$$

Since the quantity multiplying p must be greater than zero, noting that $-1 \leq \nu_{\theta z} < 1$ and rearranging yields $\nu_{r\theta} < \frac{1}{4} + \frac{E_r}{E_\theta}$, which is no more severe than the second constraint for any value of $E_z = E_\theta$.

In optimizations involving Bezier interpolation, the first constraint needed application at only the Bezier control points to ensure compliance over the entire interpolated domain. The second constraint was checked at 500 radial positions between the tendon and the bone. While the possibility exists that the second constraint was violated between these positions, this is unlikely to have occurred in any of the final solutions, as these solutions presented variations in moduli that were significant only over length scales much larger than the distance between these positions.

3. Results

3.1. A linearly graded insertion site is more effective than a non-mineralized insertion site, but less effective than a fully mineralized insertion site

We first considered the hypothetical comparison case in which the tendon was connected to the bone without an interfacial zone. In this comparison case, the radial stress at the interface between the tendon and bone rose to 1.89 times the applied stress (i.e., a stress concentration factor of 1.89) (dotted red line, Fig. 3).[1] In the comparison case where the entire insertion site was completely mineralized, the stress concentration factor was equal to 1.43 (dashed green line, Fig. 3).

The third and fourth comparison cases involved the intuitive engineering approach to reducing a stress concentration: functional grading that interpolates between the two materials. A linear grading reduced the stress concentration factor relative to the case of the unmineralized insertion site; however, the peak stress remained higher than in the case of a fully mineralized insertion site (solid blue line, Fig. 3). The fourth comparison case, a sigmoidal interpolation between the two materials, yielded a peak stress that varied as a function of the weighting ω (Fig. 4). The peak stress in this case ranged between that associated with a linear spatial grading and that associated with a sharp tendon/bone interface situated at the midpoint of the tendon-to-bone insertion site. For all four of these comparison cases, the maximum radial stress occurred at the interface of the insertion site with the bone.

3.2. A discrete, “banded” insertion site cannot improve upon a linearly graded interface

We next examined the degree to which stress concentrations are affected by a hypothetical insertion site with spatially *uniform* mechanical properties. A model of this character could eliminate the stress concentration, but only for cases in which E_r was extremely small compared to the elastic modulus of bone ($E_r < \approx 10^{-5} E_{bone}$), and small compared to E_θ (Fig.

[1]For interpretation of color in Figs. 1–7, the reader is referred to the web version of this article.

5, dark blue band along the vertical axis). The radial stress concentration dropped significantly as E_r approached zero, as observed previously for optimized functional grading of an isotropic sheet containing a hole (Huang et al., 2003).

3.3. A biomimetic distribution of mechanical properties minimizes and eliminates the radial stress concentration

A series of optimization trials were then performed to evaluate whether a smooth, continuous functional grading within the insertion site could prove more effective. $E_r(r)$, $E_\theta(r)$, and $\nu_{r\theta}(r)$ were allowed to vary independently, subject at each radial position to the thermodynamic constraints and to the physiologic constraint that neither $E_r(r)$ nor $E_\theta(r)$ could exceed E_{bone}. In the first optimization trial, $\nu_{r\theta}$ was kept constant and equal to 0.3 throughout the insertion site, leaving 28 design variables. The design variables were varied to minimize the stress concentration or, equivalently, the peak radial stress:

$$\begin{array}{ll} \min & \sigma_r^{\max}\left(E_r(r), E_\theta(r), \nu_{r\theta}(r)\right)/\sigma_{applied} \\ \text{s.t.} & 0<E_r(r) \le E_{bone}, 0<E_\theta(r) \le E_{bone}, \\ \nu_{r\theta}(r) & =0.3 \le \sqrt{E_r(r)/E_\theta(r)} \end{array} \quad (6)$$

While we could not be certain that this minimization procedure yielded a global minimum, the results proved instructive.

The result of this optimization was a complete transformation of the stress field within the model (Fig. 6, solid green line) compared to that in the insertion site with no grading or with a linear grading. At all points within the tendon, insertion site, and bone, the radial stress was lower than the applied stress. The normalized radial stress in the bone was slightly below 1, and decreased in the tendon-to-bone insertion site to a value of 0.76 close to the tendon interface.

The optimization resulted in a material property distribution qualitatively similar to that observed in the natural insertion site (Genin et al., 2009). Most notably, a compliant region in the insertion site existed in which both $E_r(r)$ and $E_\theta(r)$ dropped below the corresponding moduli of tendon. The region in which moduli of the insertion site were smaller than corresponding moduli of the tendon extended from a normalized radius $r/r_{bone} = 1.2$ to the tendon ($r/r_{bone} = 1.5$), with the minimum moduli approximately in the center of this region.

In the second optimization trial, $\nu_{r\theta}(r)$ was allowed to vary within the insertion site along with $E_r(r)$ and $E_\theta(r)$:

$$\begin{array}{ll} \min & \sigma_r^{\max}\left(E_r(r), E_\theta(r), \nu_{r\theta}(r)\right)/\sigma_{applied} \\ \text{s.t.} & 0<E_r(r) \le E_{bone}, \quad 0<E_\theta(r) \le E_{bone}, \\ & |\nu_{r\theta}(r)| \le \sqrt{E_r(r)/E_\theta(r)} \end{array} \quad (7)$$

In this case, the normalized radial stress in bone was further reduced to just 40% of the applied radial stress (Fig. 6, blue dotted line). While the stress concentration was eliminated in the case of a constant Poisson's ratio within the insertion site, including Poisson's ratio in the optimization procedure resulted in a reduction of the stresses throughout the bone and the insertion site. The moduli distributions needed to achieve such radical reduction in the radial stresses contained a biomimetic compliant band within the insertion site, in which moduli dropped below those of either the tendon or bone (Fig. 7, blue dotted line). The distribution of E_r was similar to that of the case with a constant Poisson's ratio. Compared to this previous case, the minimum value of E_θ was achieved at a point more distant from the bone than the minimum value of E_r, and the descent to this minimum was more gradual.

Poisson's ratios across the insertion site varied between −0.2 and 0.4, until a rapid rise near the insertion site/tendon interface to the tendon value of 3.

3.4. A biomimetic grading also minimizes the peak hydrostatic stress

We next asked what types of grading might reduce both principal stresses simultaneously. We repeated the optimization procedure in Eq. (6), but with the goal of minimizing the peak hydrostatic stress, $(\sigma_r + \sigma_\theta)/3$. Minimization of peak hydrostatic stress also resulted in a compliant zone analogous to Fig. 7 (results not shown). The resulting hydrostatic stress distribution was fairly uniform across the model, ranging from 0.65 to 0.74 times the applied load; for comparison, the hydrostatic stress in a homogeneous isotropic cylinder, which provides a lower bound, is 2/3 of the applied stress. In the optimum found, both radial and tangential stress concentrations were nearly eliminated: the peak stress concentration factors were 1.1 in the radial direction (bone/insertion site interface), and 1.15 in the tangential direction (tendon/insertion site interface).

4. Discussion

In the absence of the transitional tissue that forms during development, the radial stress field in an idealized model of tendon-to-bone attachment exhibits elevated stresses at the interface between tendon and bone. This stress concentration can be alleviated both by altering the interfacial material through a linear grading in mechanical properties between tendon and bone, and by altering the structure to increase the radius of the humeral head. The natural tendon to bone insertion site presents a non-monotonic grading in material properties of a character that was shown to be an improvement upon both of these strategies.

A biomimetic grading was not the only strategy for improving upon a linearly graded transition between tendon and bone. A model involving an insertion with spatially uniform mechanical properties could reduce or eliminate the radial stress concentration in tendon-to-bone attachment, but only for cases in which E_r for the "insertion site" was extremely small compared to the elastic modulus of bone ($E_r < \sim 10^{-5} E_{bone}$), and small compared to E_θ (Fig. 5, dark blue band along the vertical axis). The radial stress concentration in this model dropped significantly as E_r approached zero, as observed previously for optimized functional grading of an isotropic sheet containing a hole (Huang et al., 2003). This shielding of a stress-concentrating feature through a stiff circumferential band is analogous to the design of a porthole on a ship (Reissner and Morduchow, 1949). Note that fair comparison over the contours in Fig. 5 would involve normalization of stresses by the failure stress of tissues with the properties shown. However, this is impossible as we are uncertain whether the partial mineralization needed to obtain material properties within the insertion site strengthens or weakens tissues (Buehler, 2007; Buehler and Ackbarow, 2008).

The biomimetic grading that emerged through optimization of Bezier interpolated material properties completely eliminated the radial stress concentration (Fig. 6). The results shown are almost certainly a local minimum, as many local minima of this class were found on the way to the solution presented. While the figure shows only the best result we obtained for this particular optimization function, we emphasize that all local minima capable of eliminating the stress concentration exhibited a nominally biomimetic distribution of mechanical moduli, with the minimum radial modulus of the insertion site lower than the radial modulus of either tendon or bone. In each of the local minima for the optimization function, the modulus showed a single global minimum with respect to position analogous to that described in Genin et al. (2009). Note that the spatial distribution in radial modulus reported by Genin et al. (2009) yielded a stress concentration higher than the minimum found in our optimizations. Further, the minimum radial modulus in the physiologic insertion site is within an order of magnitude of that of tendon, while those found in our

optimizations are lower than this. This highlights the need to interpret the quantitative values emerging from this model problem with caution.

A biomimetic distribution of moduli was found to minimize concentrations in multiaxial stress state as well. The elimination of the radial stress concentration at the insertion site in the above analyses came at the expense of peak tangential stresses in excess of the applied load. The stress distribution found in optimizations aiming to minimize hydrostatic stress was very close to the equibiaxial stress field that arises within a uniform isotropic disc loaded in equibixial tension.

Poisson's ratio had a significant effect on the optimization, as it affected the way in which the insertion site transferred radial stress to tangential stress. For the case of $\nu_{r\theta} = 0.3$ throughout the insertion site, the tangential stress (results not shown) dipped close to zero within the insertion site, but rose to 1.75 times the applied radial stress near the tendon interface. Optimizing $\nu_{r\theta}$ allowed an even greater transfer of radial to tangential stress, with the peak tangential stress rising up to five times the applied load (results not shown). This is due in part to the "bump" in the radial stress distribution at $r/r_{bone} \approx 1.4$; tangential stresses are tied to the radial stress distribution through the equilibrium equations, but neither tangential stresses nor smoothness of the radial stress distribution were considered in the optimizations associated with Fig. 6.

The biomimetic distribution of moduli was not optimal for all optimization criteria. A complaint zone between tendon and bone was not advantageous in situations where radial strains and strain energy density were treated as objective functions. Minimization of peak radial strain resulted in a grading in which all elastic moduli throughout the insertion site lay between those of tendon and bone (results not shown). Minimization of strain energy density, $\frac{1}{2}\left(\sigma_r^2/E_r + \sigma_\theta^2/E_\theta - 2\nu_{r\theta}\sigma_r\sigma_\theta/E_r\right)$, resulted in a relatively flat distribution of stiffness: the majority of the optimized insertion site had elastic moduli close to that of bone, followed by an abrupt transition to the moduli of tendon. While no criteria exist at present with which to predict injury or mechanical failure within the tendon-to-bone insertion site, these results suggest that the grading observed in the rotator cuff of the humeral head might be optimized to reduce peak stresses.

While the study focused on a single anatomic region of an adult human, the results are much more general, both in the context of physiologic and engineering material attachment. When compared to the mechanical properties of bone, mechanical differences amongst tendon type, species, sex, and age are very small, and the results thus have general applicability to structural attachment of "soft" and "hard" materials.

The results provide guidance for biomimetic attachment of dissimilar materials and for surgical tendon-to-bone reattachment procedures. From the perspective of attaching engineering materials, results suggest that stresses associated with interfaces can be reduced by a biomimetic grading of elastic moduli even in cases for where no free boundary exists, for instance in the attachment of a fibrous composite component to a metallic pin (Genin and Hutchinson, 1999). From the perspective of surgical reattachment of the rotator cuff of the humeral head, results indicate that current surgical procedures, which excise transitional tissue prior to direct suturing of tendon to bone (Burkhart and Lo, 2006), might introduce higher stress concentrations into the repaired insertion site. Results further indicate that uniform scar tissue developing post-surgery, regardless of its mechanical properties, cannot return stress concentrations to physiologic levels. The physiologic grading of mechanical properties between tendon and bone thus seems a logical target for tissue engineering solutions aiming to improve surgical outcomes.

How might such a strategy be implemented? Our current efforts focus on nanofibrous networks with gradations in mineral content (Li et al., 2009) and orientation distribution (Xie et al., 2010) that mimic those of the tendon-to-bone insertion site. Such nanofibrous electrospun mats are biocompatible, and can be tailored with cues for directed cell growth (Xie et al., 2011). Although the mechanics of such structures and their long-term prospects as healing scaffolds have not yet been tested thoroughly, these studies are ongoing. Simple models for fibrous solids based upon Flory-type averaging (e.g., Marquez et al., 2005a,b, 2010) and more complicated models based upon statistical sampling of random microstructures (e.g., Gan et al., 2005; Genin and Birman, 2009) point to a wide range of mechanical properties being possible in this system, including the entire range of positive Poisson ratios found in our optimization results. However, challenges certainly lie ahead, as significant changes to stress concentrations can occur at the free boundaries of these specimens due to this anisotropy (e.g., Genin and Hutchinson, 1997, 1999) and on the interior due to inhomogeneities associated with cells (e.g., Cairns et al., 1999). These stresses in turn affect the ways that cells grow and differentiate in these model systems (Thomopoulos et al., 2011), in conjunction with what appear to be target mechanical environments and target cell concentrations (Marquez et al., 2006, 2010). Further, model systems exhibit nonlinear viscoelasticity whose character that is an ongoing subject of investigation (e.g. Pryse et al., 2003; Nekouzadeh et al., 2007).

This work highlights a physiologic strategy for reducing stress concentrations at an interface through macroscopic functional grading. Additional strategies exist over the entire range of spatial hierarchies in healthy biologic material systems (Buehler and Ackbarow, 2008). At the level of proteins, toughening mechanisms include breaking of hydrogen bonds and cross-links, unfolding of protein structures, and dissipative sliding of molecules (Buehler and Yung, 2009). For example, alpha helical protein networks have been shown to be especially efficacious in toughening protein structures (Ackbarow et al., 2009). At larger length scales within bone, sacrificial bonds of mineral between mineralized collagen fibers have been implicated in toughening (Fantner et al., 2005), as have the heterogeneous distribution and spatial density of such toughening features (Buehler, 2007; Tai et al., 2007). At still larger scales, the tendon to bone attachment exhibits interdigitation and gross morphological optimization for alleviating stress concentrations (Liu et al., 2010). The functional grading studied in this work is a promising biomimetic avenue to alleviating stress concentrations in engineering material systems, but should be understood as only one of a hierarchy of such avenues.

5. Conclusions

Using optimizations performed on an idealized model of the rotator cuff insertion site, we showed that a compliant tissue interfacial system is effective at reducing stress concentrations between tendon and bone. A band of scar tissue, as produced by current surgical techniques, cannot be as effective in reducing stress concentrations as an optimized, continuous functional grading, analogous to that which develops post-natally in the rotator cuff. Results suggest that recent biophysical characterizations of tissue mechanics at the tendon-to-bone insertion site (Genin et al., 2009) reveal an effective biomimetic strategy for joining dissimilar materials that differs fundamentally from techniques currently employed in engineering and in surgical practice.

Acknowledgments

Research support is gratefully acknowledged from the National Institutes of Health through Grants EB004347 and HL079165, from the Center for Material Innovation at Washington University. The authors thank Teresa M. Abney and Justin Lipner for discussions on interpretation of the results, and Jinhua Huang from M4 Engineering, Inc., and

Kevin Z. Truman from the University of Missouri at Kansas City for discussions of optimization procedures. Y.X.L. acknowledges a graduate fellowship from the Fannie Stevens Murphy Memorial Fund.

References

Ackbarow T, Sen D, Thaulow C, Buehler MJ. Alpha-helical protein networks are self-protective and flaw-tolerant. PLoS One. 2009; 4:e6015. [PubMed: 19547709]

Benjamin M, Kumai T, Milz S, Boszczyk BM, Boszczyk AA, Ralphs JR. The skeletal attachment of tendons – tendon "entheses". Comp. Biochem. Physiol. A: Mol. Integr. Physiol. 2002; 133:931–945. [PubMed: 12485684]

Birman V, Byrd LW. Modeling and analysis of functionally graded materials and structures. Appl. Mech. Rev. 2007; 60:195.

Blevins FT, Djurasovic M, Flatow EL, Vogel KG. Biology of the rotator cuff tendon. Orthop. Clin. North Am. 1997; 28:1–16. [PubMed: 9024427]

Buehler MJ. Molecular nanomechanics of nascent bone: fibrillar toughening by mineralization. Nanotechnology. 2007:18.

Buehler MJ, Ackbarow T. Nanomechanical strength mechanisms of hierarchical biological materials and tissues. Comput. Methods Biomech. Biomed. Eng. 2008; 11:595–607.

Buehler MJ, Yung YC. Deformation and failure of protein materials in physiologically extreme conditions and disease. Nat. Mater. 2009; 8:175–188. [PubMed: 19229265]

Burkhart SS, Lo IK. Arthroscopic rotator cuff repair. J. Am. Acad. Orthop. Surg. 2006; 14:333–346. [PubMed: 16757673]

Cairns DR, Genin GM, Wagoner AJ, Briant CL, Crawford GP. Amplified strain-rate dependence of deformation in polymer dispersed liquid crystal materials. Appl. Phys. Lett. 1999; 75:1872.

Das R, Rich J, Kim HM, McAlinden A, Thomopoulos S. Effects of botulinum toxin-induced paralysis on postnatal development of the supraspinatus muscle. J. Orthop. Res. 2011; 29:281–288. [PubMed: 20803483]

Fantner GE, Hassenkam T, Kindt JH, Weaver JC, Birkedal H, Pechenik L, Cutroni JA, Cidade GA, Stucky GD, Morse DE, Hansma PK. Sacrificial bonds and hidden length dissipate energy as mineralized fibrils separate during bone fracture. Nat. Mater. 2005; 4:612–616. [PubMed: 16025123]

Ferguson VL, Bushby AJ, Boyde A. Nanomechanical properties and mineral concentration in articular calcified cartilage and subchondral bone. J. Anat. 2003; 203(2):191–202. [PubMed: 12924819]

Fung, YC. Biomechanics: Mechanical Properties of Living Tisues. Springer; New York: 1993.

Galatz LM, Ball CM, Teefey SA, Middleton WD, Yamaguchi K. The outcome and repair integrity of completely arthroscopically repaired large and massive rotator cuff tears. J. Bone Joint Surg. Am. 2004:219–224. [PubMed: 14960664]

Gan YX, Chen C, Shen YP. Three dimensional modeling of the mechanical property of elastomeric open cell foams. Int. J. Solids Struct. 2005; 42:6628–6642.

Genin GM, Hutchinson JW. Composite laminates in plane stress: constitutive modelling and stress redistribution due to matrix cracking. J. Am. Ceram. Soc. 1997; 80(5):1245–1255.

Genin GM, Hutchinson JW. Failures at attachment holes in brittle matrix laminates. J. Compos. Mater. 1999; 33:1600–1619.

Genin GM, Kent A, Birman V, Wopenka B, Pasteris JD, Marquez JP, Thomopoulos S. Functional grading of mineral and collagen in the attachment of tendon to bone. Biophys. J. 2009; 97:976–985. [PubMed: 19686644]

Genin GM, Birman V. Micromechanics and structural response of functionally graded, particulate–matrix, fiber–reinforced composites. Int. J. Solids Struct. 2009; 46:2136–2150. [PubMed: 23874001]

Huang J, Venkataraman S, Rapoff AJ, Haftka RT. Optimization of axisymmetric elastic modulus distributions around a hole for increased strength. Struc. Multidisc. Optim. 2003; 25:225–236.

Hutchinson JW, Suo Z. Mixed mode cracking in layered materials. Adv. Appl. Mech. 1992; 29:63–191.

Lekhnitskii, SG. Anisotropic Plates. Gordon and Breach; New York: 1968.

Li X, Xie J, Lipner J, Yuan X, Thomopoulos S, Xia Y. "Nanofiber scaffolds with gradations in mineral content for mimicking the tendon-to-bone insertion site. Nano Lett. 2009; 9(7):2763–2768. [PubMed: 19537737]

Liu YX, Birman V, Chen CQ, Thomopoulos S, Genin GM. Mechanisms of bimaterial attachment at the interface of tendon to bone. ASME J. Eng. Mater. Technol. 2010; 133:8, 011006.

Lynch HA, Johannessen W, Wu JP, Jawa A, Elliott DM. Effect of fiber orientation and strain rate on the nonlinear uniaxial tensile material properties of tendon. J. Biomech. Eng. 2003; 125:726–731. [PubMed: 14618932]

Marquez JP, Elson EL, Genin GM. Whole cell mechanics of contractile fibroblasts: relations between effective cellular and extracellular matrix moduli. Philos. Trans. A: Math. Phys. Eng. Sci. 2010; 368(1912):635–654. [PubMed: 20047943]

Marquez JP, Genin GM, Zahalak GI, Elson EL. Thin bio-artificial tissues in plane stress: the relationship between cell and tissue strain, and an improved constitutive model. Biophys. J. 2005a; 88(2):765–777. [PubMed: 15596492]

Marquez JP, Genin GM, Zahalak GI, Elson EL. The relationship between cell and tissue strain in three-dimensional bio-artificial tissues. Biophys. J. 2005b; 88(2):778–789. [PubMed: 15596491]

Marquez JP, Genin GM, Pryse KM, Elson EL. Cellular and matrix contributions to tissue construct stiffness increase with cellular concentration. Ann. Biomed. Eng. 2006; 34(9):1475–1482. [PubMed: 16874557]

Matyas JR, Anton MG, Shrive NG, Frank CB. Stress governs tissue phenotype at the femoral insertion of the rabbit MCL [see comments]. J. Biomech. 1995; 28:147–157. [PubMed: 7896857]

Moffat KL, Sun WH, Pena PE, Chahine NO, Doty SB, Ateshian GA, Hung CT, Lu HH. Characterization of the structure–function relationship at the ligament-to-bone interface. Proc. Natl. Acad. Sci. USA. 2008; 105:7947–7952. [PubMed: 18541916]

Nekouzadeh A, Pryse KM, Elson EL, Genin GM. A simplified approach to quasi-linear viscoelastic modeling. J. Biomech. 2007; 40:3070–3078. [PubMed: 17499254]

Prager W. On the formulation of constitutive equations for living soft tissues. Appl. Math. 1969; 27:128–132.

Pryse KM, Nekouzadeh A, Genin GM, Elson EL, Zahalak GI. Incremental mechanics of collagen gels: new experiments and a new viscoelastic model. Ann. Biomed. Eng. 2003; 31:1287–1296. [PubMed: 14649502]

Press, WH.; Teukolsky; Saul, A.; Vetterling; William, T.; Flannery; Brian, P. Numerical Recipes: The Art of Scientific Computing. third ed. Cambridge University Press; Cambridge, UK; New York: 2007.

Reissner, H.; Morduchow, M. Reinforced Circular Cutouts in Plane Sheets. National Advisory Committee for Aeronautics; Washington, DC: 1949. Technical Note No. 1852

Stabile KJ, Pfaeffle J, Weiss JA, Fischer K, Tomaino MM. Bidirectional mechanical properties of the human forearm interosseous ligament. J. Orthop. Res. 2004; 22:607–612. [PubMed: 15099642]

Stouffer DC, Butler DL, Hosny D. The relationship between crimp pattern and mechanical response of human patellar tendon-bone units. J. Biomech. Eng. 1985; 107:158–165. [PubMed: 3999712]

Suresh, S.; Mortensen, A. Fundamentals of Functionally Graded Materials: Processing and Thermomechanical Behaviour of Graded Metals and Metal–Ceramic Composites. IOM Communications Ltd.; London: 1998.

Tai K, Dao M, Suresh S, Palazoglu A, Ortiz C. Nanoscale heterogeneity promotes energy dissipation in bone. Nat. Mater. 2007; 6:454–462. [PubMed: 17515917]

Tersoff J, LeGoues FK. Competing relaxation mechanisms in strained layers. Phys. Rev. Lett. 1994; 72:3570–3573. [PubMed: 10056233]

Thomopoulos S, Das R, Birman V, Ku K, Elson EL, Pryse KM, Marquez JP, Genin GM. Fibrocartilage tissue engineering: the role of the stress environment on cell morphology and matrix expression. Tissue Eng. Part A. 2011; 17(7–8):1039–1053. [PubMed: 21091338]

Thomopoulos S, Genin GM, Galatz LM. The development and morphogenesis of the tendon-to-bone insertion – what development can teach us about healing. J. Musculoskelet. Neuronal. Interact. 2010; 10:35–45. [PubMed: 20190378]

Thomopoulos S, Kim HM, Rothermich SY, Biederstadt C, Das R, Galatz LM. Decreased muscle loading delays maturation of the tendon enthesis during postnatal development. J. Orthop. Res. 2007; 25:1154–1163. [PubMed: 17506506]

Thomopoulos S, Marquez JP, Weinberger B, Birman V, Genin GM. Collagen fiber orientation at the tendon to bone insertion and its influence on stress concentrations. J. Biomech. 2006; 39:1842–1851. [PubMed: 16024026]

Thomopoulos S, Williams GR, Gimbel JA, Favata M, Soslowsky LJ. Variation of biomechanical, structural, and compositional properties along the tendon to bone insertion site. J. Orthop. Res. 2003; 21:413–419. [PubMed: 12706013]

Villegas DF, Maes JA, Magee SD, Donahue TL. Failure properties and strain distribution analysis of meniscal attachments. J. Biomech. 2007; 40:2655–2662. [PubMed: 17359982]

Williams ML. Stress singularities resulting from various boundary conditions in angular corners of plates in extension. J. Appl. Mech. 1952; 19:526–528.

Wopenka B, Kent A, Pasteris JD, Yoon Y, Thomopoulos S. The tendon-to-bone transition of the rotator cuff: a preliminary Raman spectroscopic study documenting the gradual mineralization across the insertion in rat tissue samples. Appl. Spectrosc. 2008; 62:1285–1294. [PubMed: 19094386]

Xie J, Liu W, Macewan MR, Yeh Y-C, Thomopoulos S, Xia Y. Nanofiber membranes with controllable microwells and structural cues and their use in forming cell microarrays and neuronal networks. Small. 2011; 7(3):293–297. [PubMed: 21294253]

Xie J, Li X, Lipner J, Manning CN, Schwartz AG, Thomopoulos S, Xia Y. Aligned-to-random nanofiber scaffolds for mimicking the structure of the tendon-to-bone insertion site. Nanoscale. 2010; 2(6):923–926. [PubMed: 20648290]

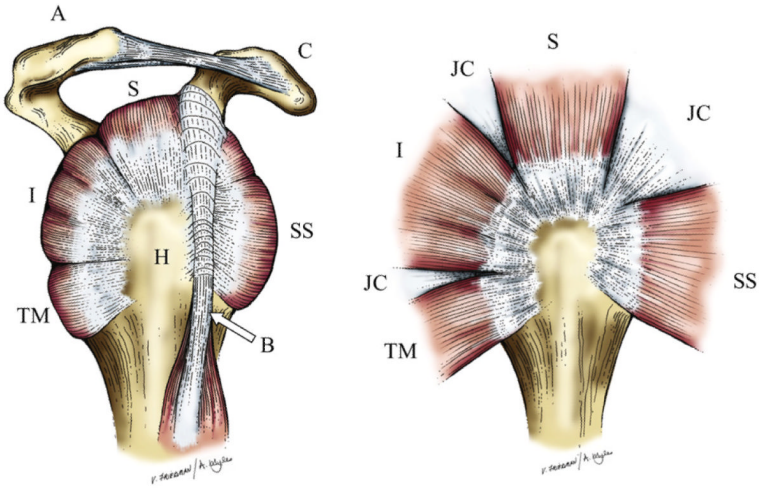

Fig. 1.

The rotator cuff as viewed from the side (i.e., the lateral view). Tendons are shown in white, muscles in red, and bones in tan. The rotator cuff tendons (TM, I, S, and SS) wrap around the spherical humeral head (H) (left panel). Removing the overlying structures (A, B, C) and unwrapping the rotator cuff tendons reveals the axisymmetric geometry of the tendons and their bony insertions (right panel).

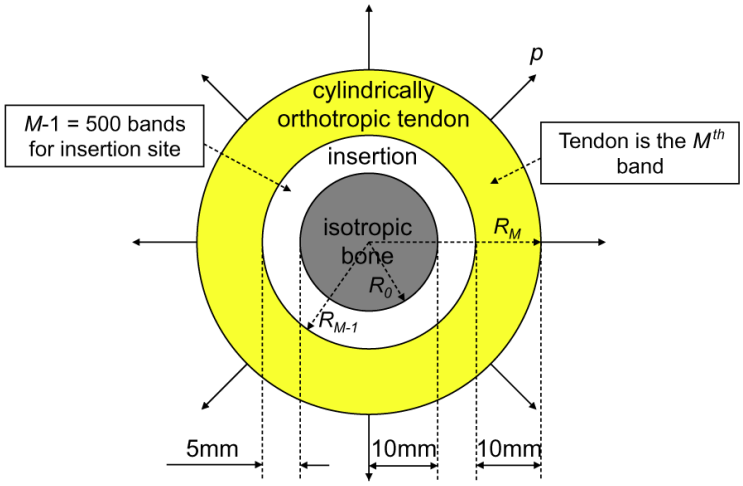

Fig. 2.

Mathematical model of an axisymmetric insertion site stressed by an equibiaxial loading, *p*. Dimensions are representative of an adult human humeral head.

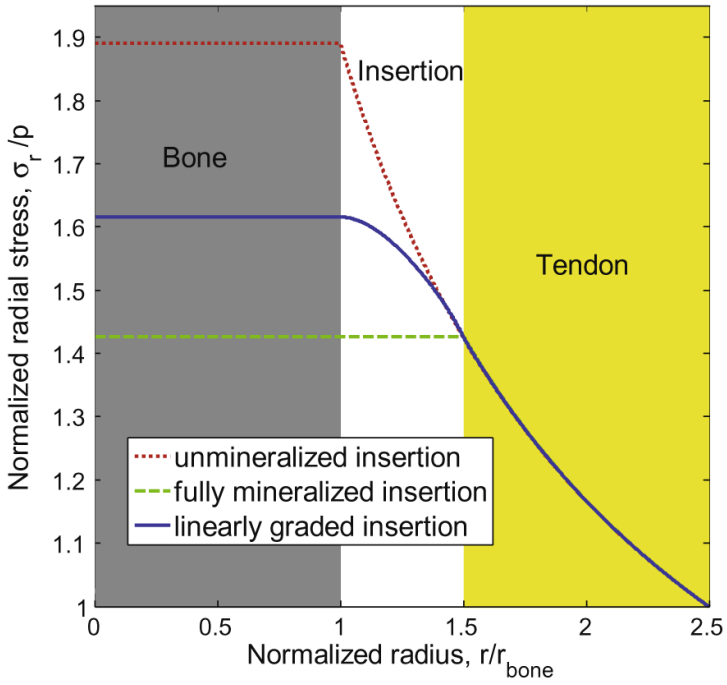

Fig. 3.
Distribution of normalized radial stress for unmineralized, fully mineralized, and linearly graded model rotator cuff insertion site.

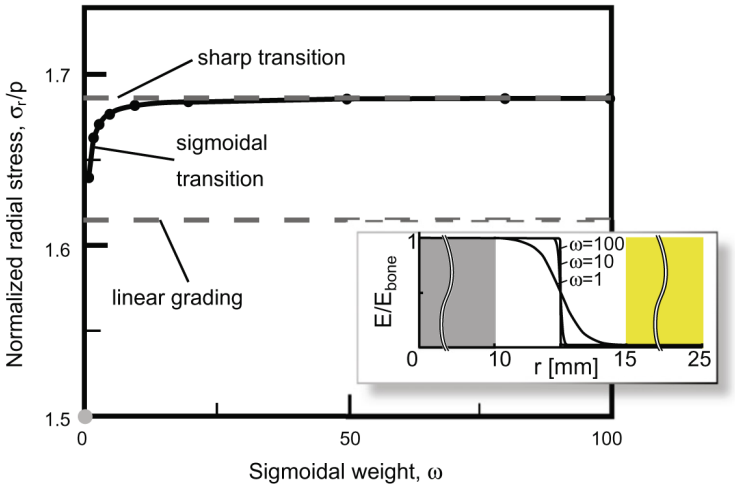

Fig. 4.

The peak stress in an insertion with sigmoidal spatial grading in elastic moduli varied, as a function of weighting ω (cf. Eq. (3)), between that associated with a linear spatial grading and that associated with a sharp tendon/bone interface situated at the midpoint of the tendon-to-bone insertion site.

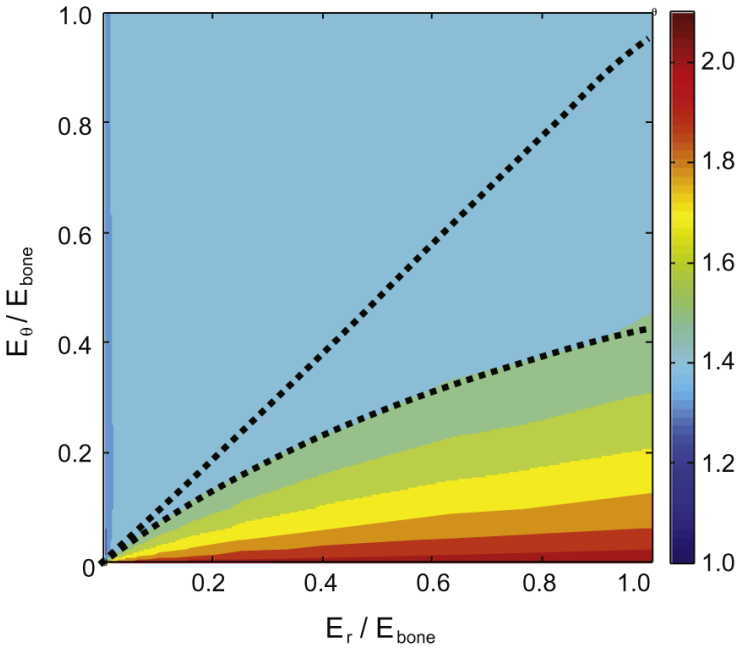

Fig. 5.

Modulation of radial stress concentration factor in a homogeneous, "three band" model of tendon to bone attachment as a function of the moduli E_r and E_θ of the middle band. At each point in the contour plot, $\nu_{r\theta}$ was optimized to minimize radial stress concentrations. Above the upper dotted line (upper left), the peak radial stress occurred at the tendon/insertion site interface or within the tendon; for the region below the lower dotted line, the peak stress occurred at the tendon/bone interface; at points in between, the peak stress occurred within the insertion site.

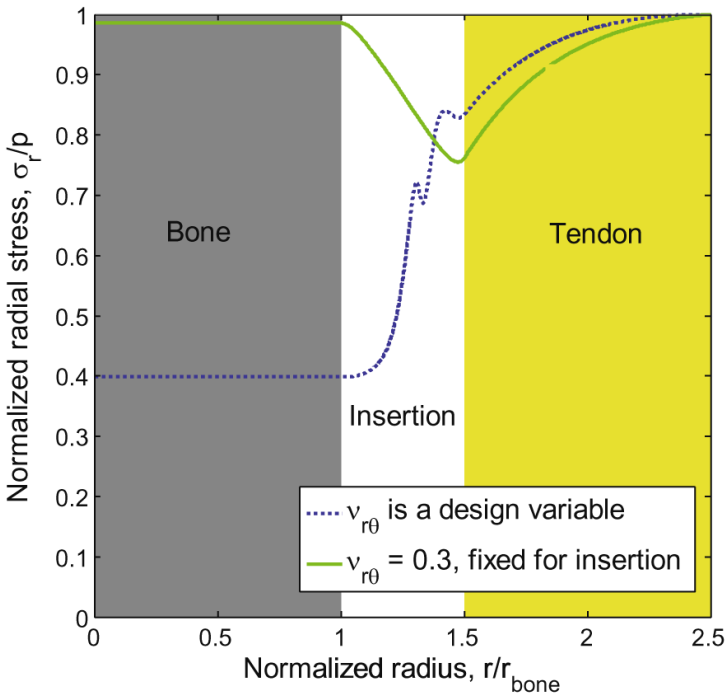

Fig. 6.
Distribution of normalized radial stress in an insertion site optimized to minimize stress concentration factor. In both cases, the stress concentration was eliminated. Note that the irregular peaks in the blue line could not be controlled: the optimization criterion was not influenced by local peaks.

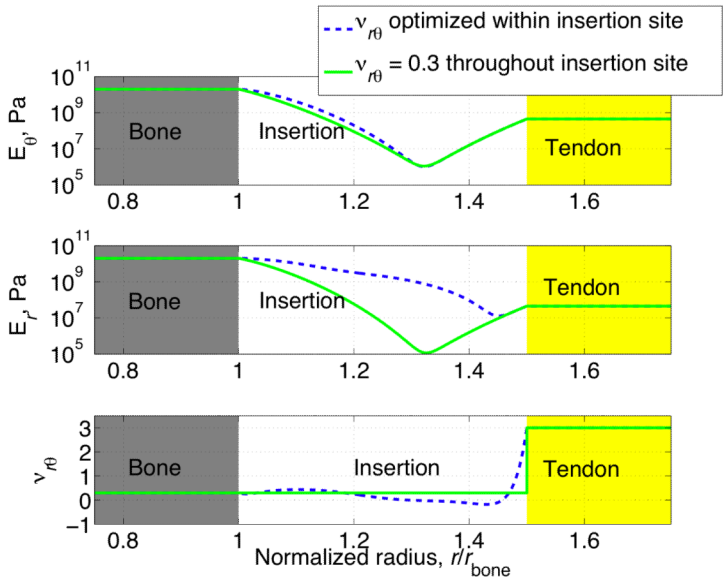

Fig. 7.

The distribution of material properties for minimization of radial stress concentration factor contains a biomimetic compliant band between tendon and bone. Results for minimization of a multiaxial (hydrostatic) stress (not shown) are analogous. Allowing Poisson's ratio to vary across the insertion site had strong effect on the optimum distribution of tangential elastic modulus, but little effect on the optimum distribution of radial elastic modulus.